applied sciences

MDPI

Article

Evaluation of Specific Absorption Rate in Three-Layered Tissue Model at 13.56 MHz and 40.68 MHz for Inductively Powered Biomedical Implants

Krithikaa Mohanarangam, Yellappa Palagani and Jun Rim Choi *

School of Electronics Engineering, College of IT Engineering, Kyungpook National University, Daegu 702-701, Korea; krithikaamohan@gmail.com (K.M.); palaganiyellappa@gmail.com (Y.P.)

* Correspondence: jrchoi@knu.ac.kr; Tel.: +82-053-950-6567

Received: 1 February 2019; Accepted: 11 March 2019; Published: 17 March 2019

Abstract: This paper presents an optimized 3-coil inductive wireless power transfer (WPT) system at 13.56 MHz and 40.68 MHz to show and compare the specific absorption rate (SAR) effects on human tissue. This work also substantiates the effects of perfect alignment, lateral and/or angular misalignments on the power transfer efficiency (PTE) of the proposed WPT system. Additionally, the impacts of different tissue composition, input power and coil shape on the SAR are analyzed. The distance between the external and implantable coils is 10 mm. The results have been verified through simulations and measurements. The simulated results show that the SAR of the system at 40.68 MHz had crossed the limit designated by the Federal Communications Commission and hence, it is unsafe and causes tissue damage. Measurement results of the system in air medium show that the optimized printed circuit board coils at 13.56 MHz achieved a PTE of 41.7% whereas PTE waned to 18.2% and 15.4% at 10 mm of lateral misalignment and 60° of angular misalignment respectively. The PTE of a combination of 10 mm lateral misalignment and 60° angular misalignment is 21%. To analyze in a real-environment, a boneless pork sample with 10 mm of thickness is placed as a medium between the external and implantable coils. At perfect alignment, the PTE through pork sample is 30.8%. A RF power generator operating at 13.56 MHz provides 1 W input power to the external coil and the power delivered to load through the air and tissue mediums are 347 mW and 266 mW respectively.

Keywords: implantable medical devices; 3-coil inductive link; power transfer efficiency; air medium and tissue medium; specific absorption rate

1. Introduction

Implantable devices with wireless connectivity has led to many advances in the field of biomedical applications, as they allow long term powering of devices within the human body [1–6]. The principal power required by the medical implants such as cochlear implants, retinal prostheses, pacemakers, and neural recordings are different [7–9] and therefore powering these devices without damaging the tissues remain an arduous challenge. The conventional techniques used physical wirings and batteries to provide power to the implantable medical devices (IMDs). However, the probability of wires getting tangled is high and the batteries are larger in size and have a shorter span [10,11]. These drawbacks of the conventional techniques result in surgical complications and infections. By employing wireless power transfer (WPT) technology in IMDs, we can potentially reduce the risk of infection and patient's discomfort.

The 2-coil inductive link with transmitter and receiver coils is the most popular conventional method for wirelessly transferring power to biomedical implants [1,12]. This system can transfer power only over a relatively short distance. In the recent past [2], the 4-coil resonance-based link operating in the midfield region was considered to be the efficient alternative to 2-coil inductive link as using the 4-coil resonance-based link increases the overall power transfer efficiency (PTE) of the system. However, the main drawback of the 4-coil resonance-based link is that the method increases the PTE by reducing the power delivered to the load (PDL). Instead, a 3-coil inductive link proposed in [13–15], provides a higher PTE without reducing the PDL. Figure 1a–c show the block diagrams of 2-coil, 3-coil and 4-coil links respectively.

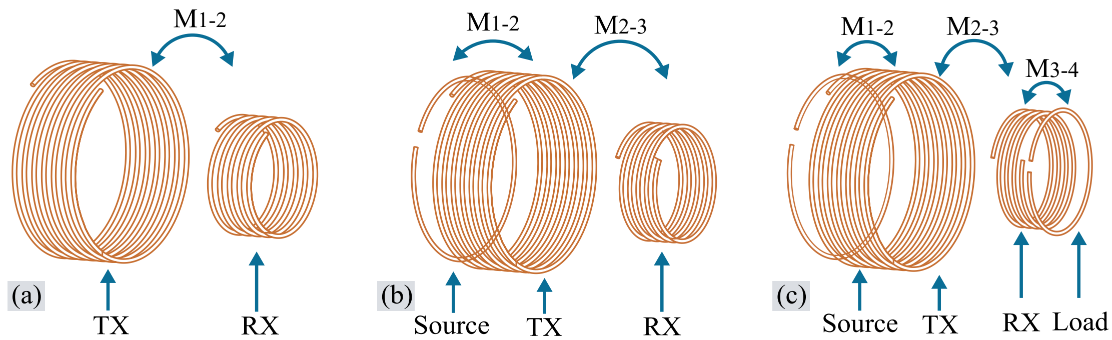

Figure 1. Block diagram of (**a**) 2-coil; (**b**) 3-coil; (**c**) 4-coil WPT systems.

One of the key challenges in designing a WPT system for biomedical applications is to attain a maximum PTE without contravening the specific absorption rate (SAR) limits established by the Federal Communications Commission (FCC) [16]. A significant amount of research has been dedicated to the goal of designing a small-sized implant in optimal frequency range. The size of the implantable coil operating in the sub-gigahertz to low-gigahertz frequencies is typically between 1 to 2 mm [17,18] and the size of the implantable coil can be increased by curtailing the frequency [4,19]. The commonly suggested optimal operating frequency (f_0) for designing mm-sized coils to achieve higher PTE is above 100 MHz [20]. Despite the fact that the system achieves a higher PTE with mm-sized coil at $f_0 \geq 100$ MHz, a frequency higher than 20 MHz can adversely affect the tissues of human due to high electromagnetic radiations [10,21]. So, in this paper, a 3-coil inductive link with a small-sized circular implant at a distance of 10 mm from the circular shaped external coil is designed to investigate the effects of low and high industrial, scientific, and medical (ISM) frequencies on SAR in tissue medium. 13.56 MHz is considered as a low ISM frequency in the near-field domain as it is FCC approved for industrial and medical applications and 40.68 MHz is considered as a high ISM frequency as it is more than the prescribed FCC limit. Additionally, the simulated SAR is analyzed with respect to different tissue composition, input power, and coil shape at 13.56 MHz and 40.68 MHz.

The remaining paper is organized as follows: the equivalent structure of a 3-coil inductive link and orientation of the coils are discussed in Section 2. Design procedure and simulation results are presented in Section 3. Section 4 shows the measurement results, followed by the conclusion in Section 5.

2. Equivalent Circuit Model and Orientation Analysis of a 3-Coil Inductive Link

The 3-coil WPT link is an extension of the conventional 2-coil WPT link. The equivalent circuit of the 3-coil system is shown in Figure 2, where L_1, L_2 and L_3, denote the source, transmitter, and receiver coils respectively. The source L_1 is added either to the high-Q transmitter coil L_2 or receiver coil L_3 [22,23]. In general, for bio-medical applications, the L_1 is added to the L_2 to minimize the size and complexity of the implanted unit and to optimize the system even after implantation [24]. The L_1 and L_2 are strongly coupled to each other and in turn are mutually coupled with the L_3. C_1, C_2 and C_3 are the resonant capacitances of L_1, L_2 and L_3 respectively and are placed in series with the coils. R_1, R_2 and R_3 are the self resistances of L_1, L_2 and L_3 respectively. R_S, R_L, P_{in} and P_{out} are the source resistance, load resistance, input and output power of the system respectively. The Equations (1)–(3) represent the mutual inductance (M_{ab}), quality factor (Q_{ab}), and PTE of the system [10,25].

$$M_{ab} = k_{ab}\sqrt{L_a L_b} \qquad (0 < k < 1) \tag{1}$$

$$Q_{ab} = f_r/\Delta_f \tag{2}$$

$$\mathrm{PTE} = |\mathrm{S}_{21}{}'|^2 \times 100(\%) \tag{3}$$

where $a, b \in \{1,2,3\}$, k_{ab} is the coupling coefficient between the coils a and b, L_a and L_b are the self-inductance of the coils a and b, f_r and Δf are the resonance frequency and resonance bandwidth of the WPT system and S_{21} is the linear magnitude of the transmission coefficient.

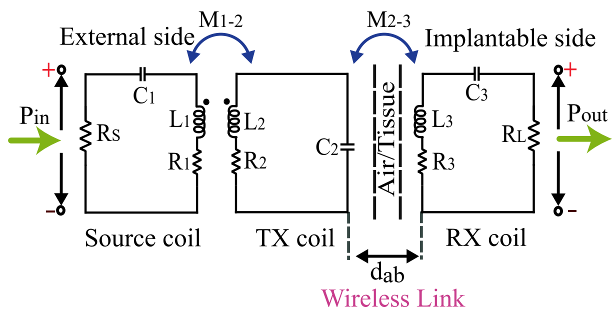

Figure 2. The equivalent circuit model of a 3-coil inductive link.

The PTE of the WPT system is influenced by the M_{ab} and Q_{ab}, which in turn depend on the position and geometry of the external and implantable coils [10,26]. In this paper, the external and implantable coils have a circular shape and are exposed to alignment conditions, namely perfect alignment, lateral and/or angular misalignments. In perfect alignment, the external and implantable coils remain parallel to each other and their center points are collinear. In lateral misalignment, the external and implantable coils remain parallel to each other, but the center of the implantable coil is displaced by a distance δ. In angular misalignment, the implantable coil tilts from its ideal position and forms an angle α. In the case where both lateral and angular misalignments are present, the implantable coil endures a shift in the axial position in addition to the rotation. The coordinates of the circular shaped coils are

$$x_c = rcos\varphi; \quad y_c = rsin\varphi; \quad z_c = 0$$

where x_c, y_c, and z_c are the cartesian coordinates of circular shaped coil and r is the radius of the external/implantable coil. The coordinates of the coils at various alignment conditions are presented in Table 1 and Figure 3a.

Table 1. The implantable coil under perfect and misalignment cases with respect to external coil [27].

Alignment Cases	External Coil	Implantable Coil
Perfect alignment	(x_c, y_c, z_c)	$(x_c, y_c, z_c{+}d_{ab})$
Lateral misalignment	(x_c, y_c, z_c)	$(x_c, y_c{+}\delta, z_c{+}d_{ab})$
Angular misalignment	(x_c, y_c, z_c)	$\begin{bmatrix} 1 & 0 & 0 \\ 0 & cos\theta & -sin\theta \\ 0 & sin\theta & cos\theta \end{bmatrix} \begin{bmatrix} x_c \\ y_c \\ z_c + d_{ab} \end{bmatrix}$
Angular and lateral misalignments	(x_c, y_c, z_c)	$\begin{bmatrix} 1 & 0 & 0 \\ 0 & cos\theta & -sin\theta \\ 0 & sin\theta & cos\theta \end{bmatrix} \begin{bmatrix} x_c \\ y_c + \delta \\ z_c + d_{ab} \end{bmatrix}$

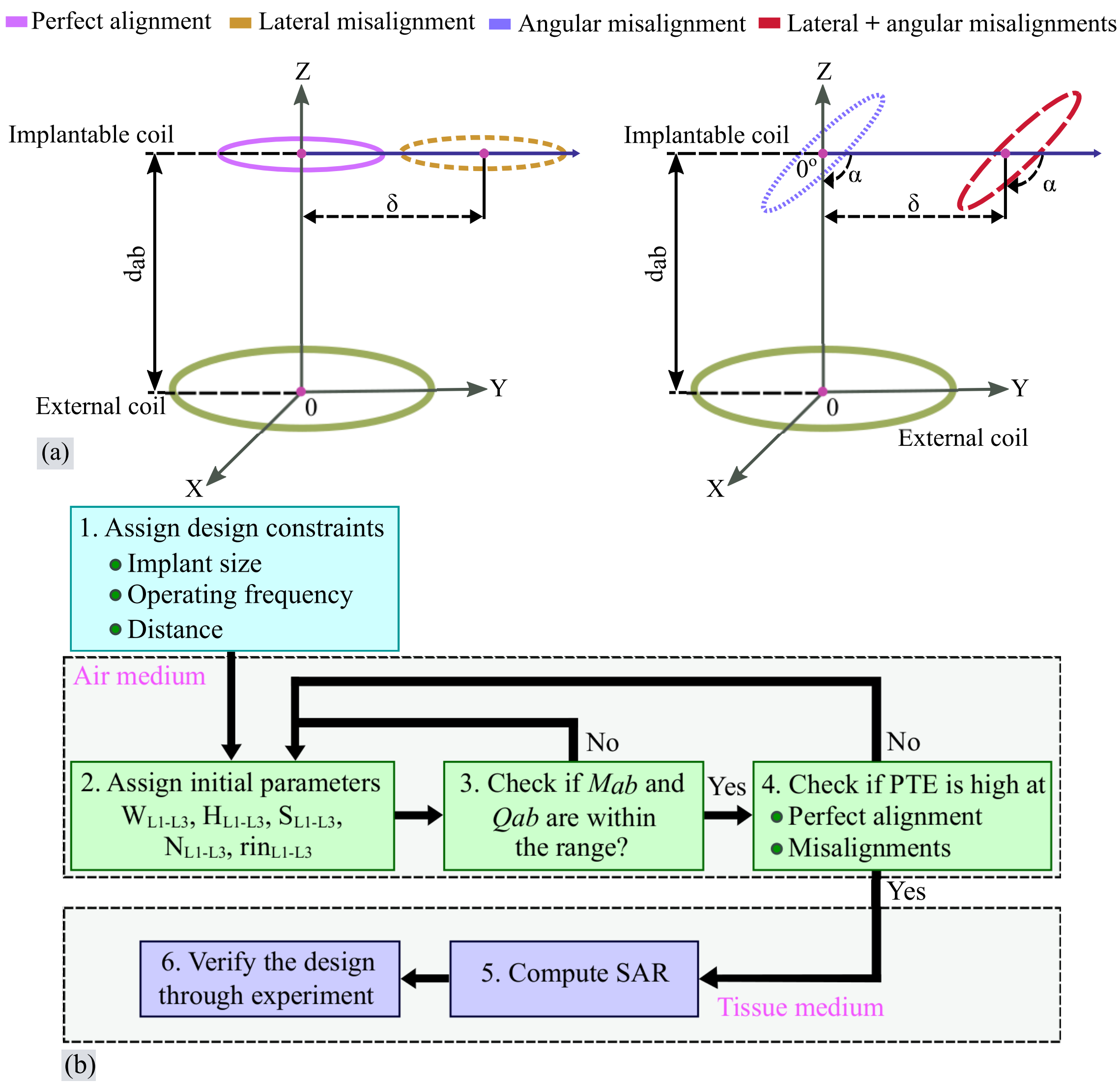

Figure 3. (**a**) Orientation of the external and implantable coils; (**b**) Flowchart of the optimization procedure of a 3-coil inductive link.

3. Design Procedure and Simulation Results

The procedure for designing the 3-coil inductive link is shown in Figure 3b. Firstly, the procedure begins with optimizing the design parameters that aids in achieving a high PTE. The external and implantable coils of the 3-coil inductive link is designed using the obtained optimized parameters at 13.56 MHz and 40.68 MHz to investigate the effects of low and high ISM band frequencies on the human tissue model. This iterative design procedure is carried out by the high frequency structure simulator (HFSS) and the input power is set to 1 W.

Step 1: Assign Design Constraints: The implant size, operating frequency, and distance between the coils are the main constraints to design the 3-coil inductive link. These design constraints are assigned and optimized based on the application and printed circuit board (PCB) fabrication process.

Step 2: Assign the Initial Parameters: The initial parameters which are assigned and optimized for designing the 3-coil inductive link are copper wire width ($W_{L_1-L_3}$), copper wire height ($H_{L_1-L_3}$), spacing between the wires ($S_{L_1-L_3}$), number of turns of a coil ($N_{L_1-L_3}$), and inner radius of the coil ($r_{inL_1-L_3}$). The initial parameter $H_{L_1-L_3}$ are assigned considering the PCB fabrication constraints.

Step 3: M_{ab} and Q_{ab}: The M_{ab} and Q_{ab} of the coils play a vital role in achieving a higher PTE. The M_{ab} and Q_{ab} depend on the initial parameters and therefore optimizing the initial values lead to a high M_{ab} and Q_{ab}. The C_1, C_2 and C_3 are 100 pF, 423 pF, and 300 pF respectively, and the resistors R_S and R_L are set to 50 Ω each. If the resulting M_{ab} is low and Q_{ab} lies outside the expected range, then the initial parameters are optimized further to achieve a high PTE [2,28]. At f_0 = 13.56 MHz, M_{ab} = 905.1 nH and Q_{ab} = 25.3 and at f_0 = 40.68 MHz, M_{ab} = 2516.6 nH and Q_{ab} = 15. Figure 4a,b shows the M_{ab} with respect to d_{ab} at 13.56 MHz and 40.68 MHz and Figure 4c,d shows the Q_{ab} with respect to resonance frequency at 13.56 MHz and 40.68 MHz.

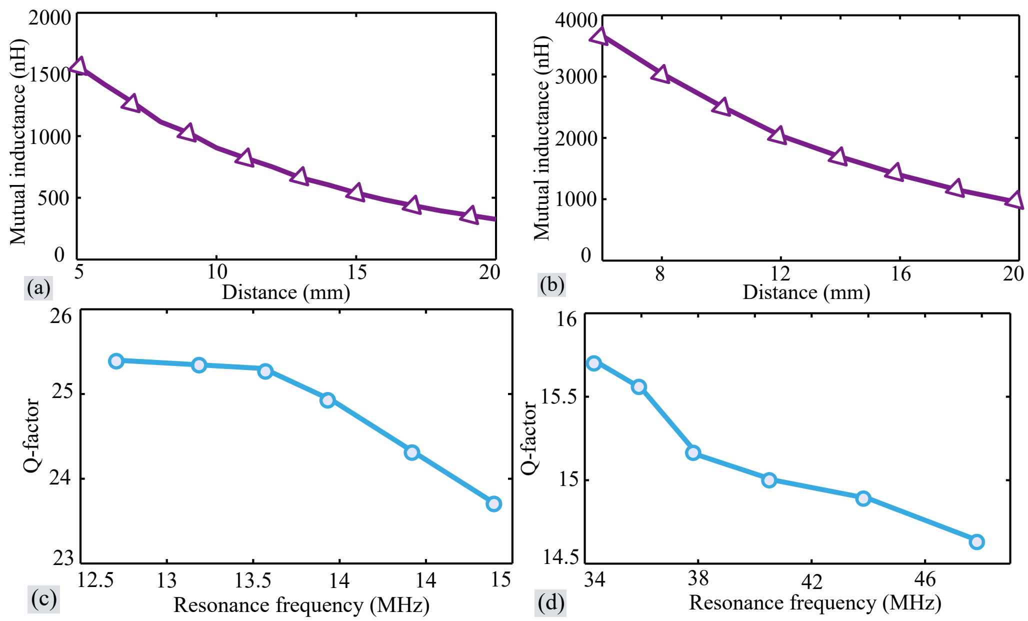

Figure 4. (**a**) Mutual inductance vs. distance between the coils at 13.56 MHz; (**b**) Mutual inductance vs. distance between the coils at 40.68 MHz; Q-factor vs. resonance frequency at (**c**) 13.56 MHz operating frequency; (**d**) 40.68 MHz operating frequency.

Step 4: PTE: This step discusses the effects of W_{L_3} and N_{L_3} on PTE as one of the applications of this paper is to design an implantable coil less than 2 cm. The PTE is evaluated based on the optimal design parameters obtained above and for a low PTE, *step*-2 is repeated iteratively as optimizing the initial parameters ameliorates the M_{ab} and Q_{ab}, thereby increasing the PTE of the system. At perfect alignment, the maximum PTE achieved with W_{L_3} = 0.3 mm and N_{L_3} = 10 for 10 mm d_{ab} and 13.56 MHz is 53.3%. The same iterative procedure is repeated at 40.68 MHz and at perfect alignment, the system achieved a maximum PTE of 70.8% with W_{L_3} = 0.8 mm and N_{L_3} = 6. Figure 5a,b show the change in PTE with respect to distance at 13.56 MHz and 40.68 MHz respectively. The results show that the PTE decreases gradually with increasing d_{ab}. Table 2 presents the final optimized values of the design examples at 13.56 MHz and 40.68 MHz. Generally, the PTE declines under misalignment conditions, so, the system is also analyzed under lateral and/or angular misalignments.

1. *Lateral Misalignment*: The implantable coil is laterally displaced from a perfectly aligned position of 0 mm to 10 mm. The system has been simulated at laterally displaced misalignment positions of 5 mm and 10 mm. At 13.56 MHz with a maximum misaligned distance of 10 mm, the PTE is 30.2% whereas at 40.68 MHz with a maximum misaligned distance of 10 mm, the PTE is 49.2%.
2. *Angular Misalignment*: In order to validate the effects of angular misalignment on the PTE, the implantable coil is rotated through angles 15°, 30°, 45°, and 60° relative to the external coil. At 13.56 MHz, when α = 15°, the PTE is 52.3% and with the increase of angular misalignment the PTE declines sharply, and the PTE is 29.4% at α = 60°. At 40.68 MHz, when α = 15°, the PTE is 65.1% and at α = 60°, the PTE is 42.1% .
3. *Combination of Lateral and Angular misalignment*: Here, the PTE is tested for misalignment angles 0° to 60° along with laterally displaced positions 1 mm to 10 mm. At 60° angular rotation and 10 mm lateral displacement, the PTE at 13.56 MHz and 40.68 MHz are 39.1% and 57.6% respectively. The overall PTE under perfect alignment, lateral and/or angular misalignments are shown in Figure 5c,d. The proposed geometry of the coils are shown in Figure 6.

Table 2. Optimized geometries for proposed coil designs.

Coils	PCB Parameter	f_0 = 13.56 MHz	f_0 = 40.68 MHz
L_1	r_{inL_1}(mm)	25.5	35.95
	r_{outL_1}(mm)	27.5	38.05
	W_{L_1}(mm)	2	2.1
	H_{L_1}(mm)	0.07	0.07
	N_{L_1}	1	1
L_2	r_{inL_2}(mm)	4.75	5.07
	r_{outL_2}(mm)	22.45	23.42
	W_{L_2}(mm)	1.5	0.85
	H_{L_2}(mm)	0.07	0.07
	S_{L_2}(mm)	1.2	0.9
	N_{L_2}	6	10
L_3	r_{inL_3}(mm)	0.45	0.45
	r_{outL_3}(mm)	9.95	9.95
	W_{L_3}(mm)	0.3	0.8
	H_{L_3}(mm)	0.07	0.07
	S_{L_3}(mm)	0.62	0.65
	N_{L_3}	10	6

Step 5: SAR at Tissue Medium: The SAR is a number that measures the rate at which energy is absorbed by the human body when exposed to electromagnetic radiations. According to FCC, a SAR level of less than 1.6 W/kg is considered safe and therefore it is important to make sure that the frequency absorbed by human tissue does not exceed this level. The SAR is defined by [10,29]

$$SAR = \sigma|E|^2/\rho$$

where σ is the tissue conductivity, E is the intensity of electric field, and ρ is the human tissue density.

The SAR cannot be measured experimentally and therefore the SAR of the system is simulated at 13.56 MHz and 40.68 MHz using HFSS. The implantable coil is usually placed in less than 10 mm of depth in human tissue. So, to analyze the design in this realistic environment, the human tissue model is formed using three consecutive layers of 1 mm skin, 2 mm fat and 7 mm muscle. Table 3 shows the dielectric properties of the layers to be used for constructing the model. At 13.56 MHz, the PTE and SAR are 48.2% and 0.91 W/kg respectively, whereas at 40.68 MHz, the PTE and SAR are 55.7% and 5.0 W/kg respectively.

Though at 40.68 MHz the PTE is high, the SAR had crossed 1.6 W/kg, the limit designated by the FCC and hence, it is unsafe and causes tissue damage. Figure 7a,b shows the change in PTE with respect to the distance between the coils at 13.56 MHz and 40.68 MHz respectively. For an input power of 1 W, the simulated SAR value at 13.56 MHz and 40.68 MHz are shown in Figure 7c,d respectively.

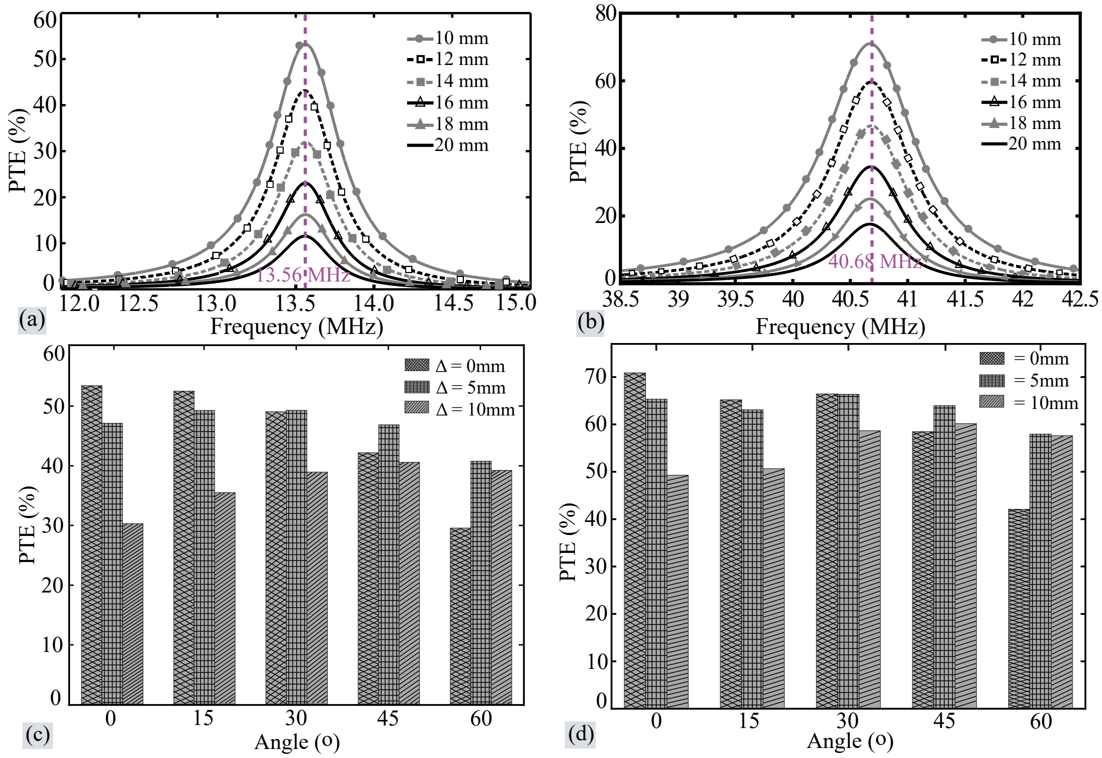

Figure 5. (**a**) PTE vs. frequency vs. distance at 13.56 MHz; (**b**) PTE vs. frequency vs. distance at 40.68 MHz; PTE vs. alignment configurations at (**c**) 13.56 MHz; (**d**) 40.68 MHz.

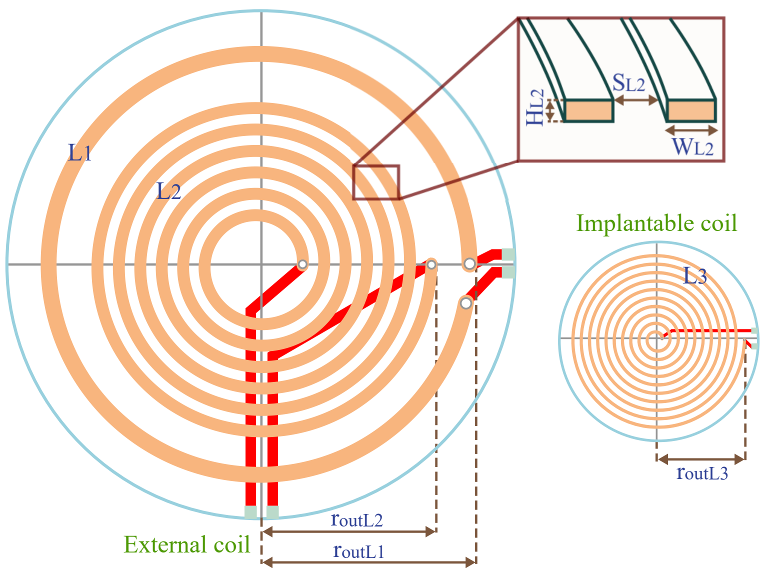

Figure 6. Proposed geometry coil types.

Table 3. The dielectric properties of the human body tissue at 13.56 MHz and 40.68 MHz [30].

Parameters	Frequency (MHz)	Dry Skin	Wet Skin	Fat	Muscle
Conductivity [S/m]	13.56	0.23802	0.38421	0.030354	0.62818
	40.68	0.37982	0.45519	0.034136	0.66986
Relative permittivity	13.56	285.25	177.13	11.827	138.44
	40.68	122.91	92.985	7.286	82.115
Loss tangent	13.56	1.1062	2.8754	3.4021	6.0152
	40.68	1.3655	2.1631	2.0703	3.6046

Additionally, the effects of different compositions of tissue, input power and coil shape on the SAR is analyzed. The percentage of skin, fat and muscle varies from person to person, therefore, in addition to 1 mm of skin, 2 mm of fat and 7 mm of muscle, the human tissue model is also formed using 1.5 mm of skin, 2.5 mm of fat and 6 mm of muscle and 2 mm of skin, 3 mm of fat and 5 mm of muscle. Figure 7e,f show the effects of different tissue composition on SAR.

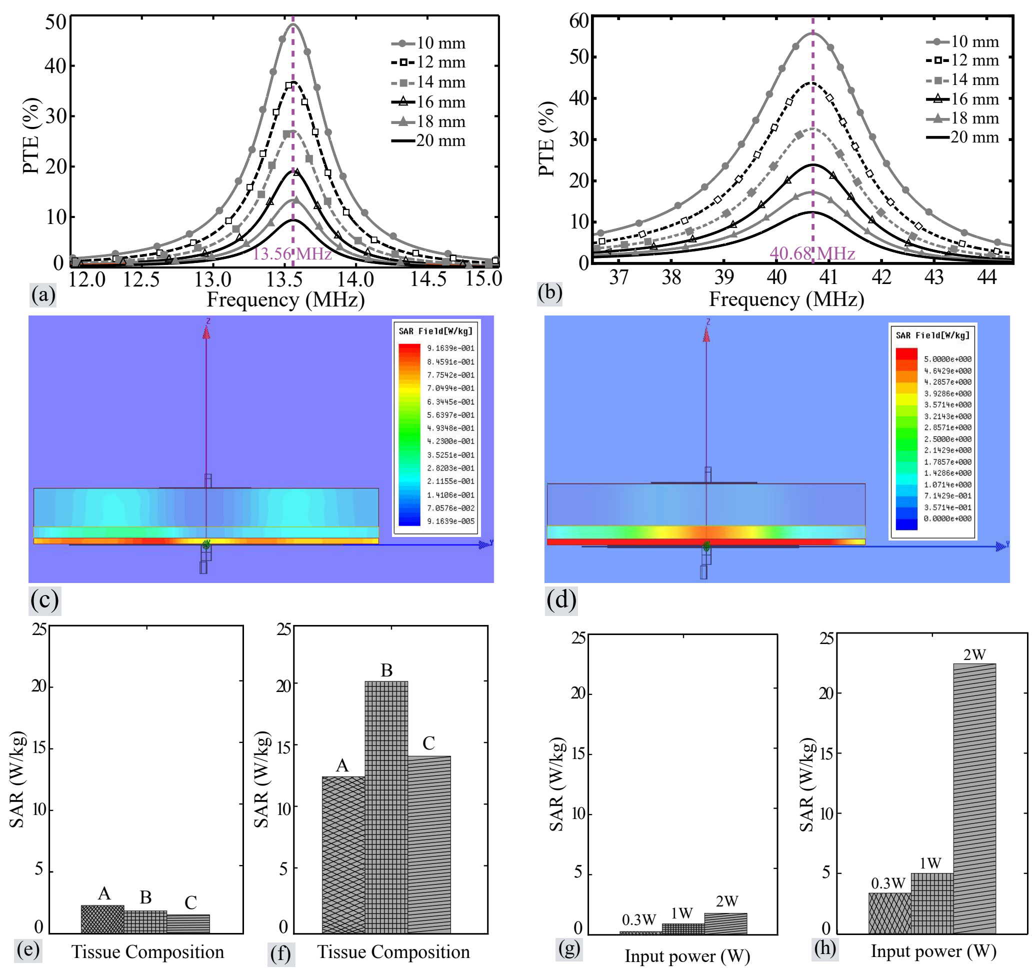

Figure 7. (**a**) PTE vs. frequency for varied distances at 13.56 MHz; (**b**) PTE vs. frequency for varied distances at 40.68 MHz; (**c**) Simulated SAR at 13.56 MHz; (**d**) Simulated SAR at 40.68 MHz (**e**) SAR vs. Tissue Composition at 13.56 MHz. (**f**) SAR vs. Tissue Composition at 40.68 MHz (**g**) SAR vs. Input power at 13.56 MHz. (**h**) SAR vs. Input power at 40.68MHz (A: 1 mm skin, 2 mm fat and 7 mm muscle, B: 1.5 mm skin, 2.5 mm fat and 6 mm muscle, and C: 2 mm skin, 3 mm fat and 5 mm muscle).

To analyze the effects of input power on SAR, in addition to 1 W, the system is also simulated with input powers of 0.3 W and 2 W at 13.56 MHz and 40.68 MHz. Figure 7g,h depicts the change in SAR value with respect to the input power at 13.56 MHz and 40.68 MHz respectively. From Figure 7g,h, the analysis shows that the SAR value increases with increase in input power. For an input power of less than 2 W, the SAR produced is below the limit set by FCC at 13.56 MHz, but, at 40.68 MHz, the SAR exceeds the limit set by FCC for a low input power of 0.3 W.

To analyze the impacts of coil shape on SAR, a system with circular shaped external and spherical shaped implantable coils is simulated with an input of 1 W at 13.56 MHz and 40.68 MHz [31]. The SAR value at 13.56 MHz and 40.68 MHz are 0.29 W/kg and 3.60 W/kg respectively. From the results, it can be observed that the SAR value at low frequency is small when compared to high frequency irrespective of the shape of the coil.

Step 6: End of Optimization Procedure: The proposed 3-coil WPT system designed through simulation is validated by experiments.

4. Measurement Results

The experimental setup is designed and implemented to validate the simulated results obtained in Section 3. The L_1, L_2 and L_3 are fabricated using PCB technique from copper with the same height and variable widths. As shown in Figure 8a,b, L_1, L_2 and L_3 are fabricated from copper with a width of 1.9 mm, 1.5 mm, and 0.3 mm respectively and a height of 0.07 mm. The PTE of the 3-coil inductive link through the air and tissue mediums are measured using two experimental setups shown in Figure 8c,d.

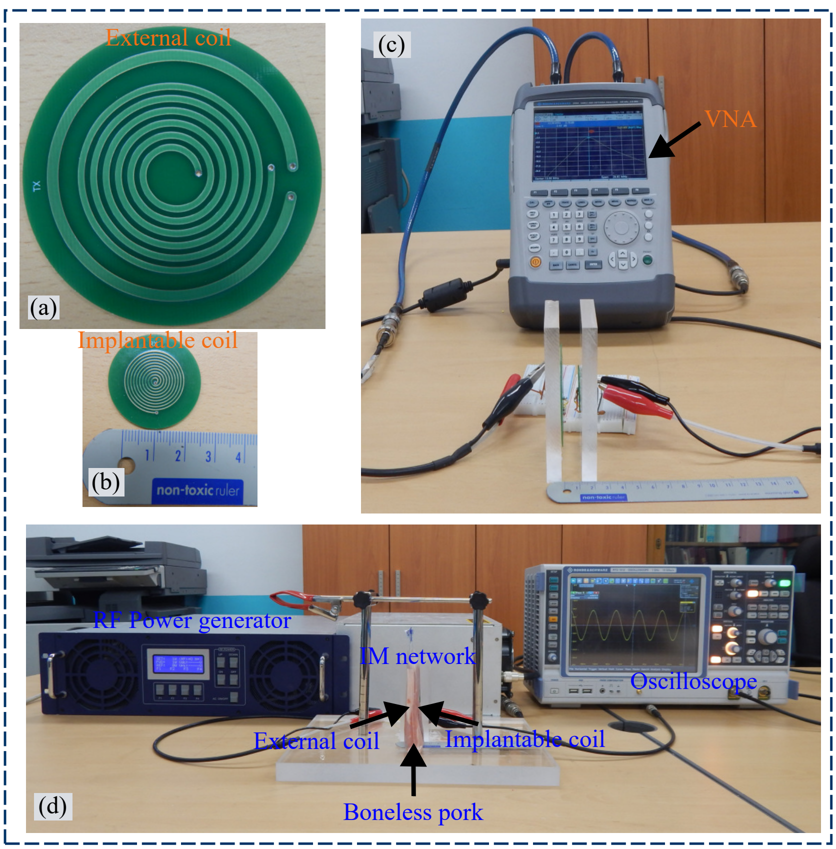

Figure 8. Fabrication of (**a**) External coil; (**b**) Implantable coil; (**c**) Experimental setup for measuring the PTE; (**d**) Experimental setup for measuring the PDL.

The first method is to measure S_{21} parameter through the air and tissue mediums by connecting L_1 to port 1 and L_3 to port 2 of a vector network analyzer (VNA). The ports 1 and 2 of the VNA are connected to an impedance of 50 Ω each. The distance between the external and implantable coils is set to 10 mm at air and tissue mediums. The PTE of the 3-coil inductive link through the air at perfect alignment, lateral misalignment, angular misalignment and a combination of lateral and angular misalignment are 41.7%, 18.2%, 15.4% and 21% respectively. To check the PTE in tissue environment, a boneless pork sample with 10 mm of thickness is placed as a medium between the external and implantable coils. At perfect alignment, the PTE through pork sample waned to 30.8%.

We have measured the link efficiency using VNA in order to compare it to the simulated transmission coefficient (S_{21}). However, we cannot measure the actual amount of power received by the receiver coil using VNA. Thus, a second method as shown in Figure 8d is used to measure the received power. This method is used to measure the actual amount of power transferred from L_1 and L_2 to L_3. The RF power generator is connected to the impedance matching (IM) network to create a matched frequency between the external and implantable coils. Generally, the capacitances are varied to tune the resonance frequency to operating frequency. However, in practical applications, it is not possible to vary the values of the capacitance. So, in this paper, we have used IM network to tune the resonance frequency to the operating frequency. Auto tuning the IM network allows the design to achieve the maximum PTE in the air or tissue medium as IM network tunes till it achieves the minimum power reflected. The minimum power is reflected only when the resonance frequency of the coil is equal to the operating frequency. Therefore, the resonance frequency can be tuned to operating frequency in the air and tissue mediums.

At 13.56 MHz, the impedance network sends an input of 1 W received from the RF generator to the external coil and the output on the implantable side is measured in terms of voltage and current through an oscilloscope. At a distance of 10 mm from the external coil, the implantable coil at perfect alignment received power of 347 mW and 266 mW (in terms of PTE: 34.7% and 26.6%) in the air and tissue mediums respectively. It can observed that the PTE measured is less than S_{21}. The proposed work is compared with the conventional works in terms of PTE with respect to coil size, operating frequency and distance between the coils. The results are summarized in Table 4.

Table 4. Comparison with the Conventional Works.

Ref.	Type of Wireless Link	Tech.	RX Coil Diameter (mm)	Operating Frequency (MHz)	Distance (mm)	Medium	PTE (%)
[32]	2-coil	PSC	10 × 10	13.56	10	Air Saline Tissue	72.2 51.8 30.8
[33]	2-coil	PCB	25 × 10	13.56	10	Air Tissue	75 58.2
[34]	4-coil	PCB	5 × 5	13.56	10	Air Tissue	19.1 11.7
[29]	2-coil	-	10.8 × 10.5	39.86	10	Tissue	47.2
This work	3-coil	PCB	19.9	13.56	10	Air Tissue	41.7 30.8

5. Conclusions

In this paper, a 3-coil inductive WPT system with a small-sized implantable coil is designed and simulated by HFSS to investigate and compare the SAR distribution at 13.56 MHz and 40.68 MHz. The impacts of perfect alignment, lateral and/or angular misalignments on the PTE of the 3-coil inductive WPT system have also been analyzed. Additionally, the effects of different compositions of tissue, input power, and coil size on the SAR is analyzed. For an input power of less than 2 W, the SAR produced is below the limit set by FCC at 13.56 MHz, but, at 40.68 MHz, the SAR exceeds the limit set by FCC for a low input power of 0.3 W. An analysis on the impact that various coil shapes have on SAR shows that irrespective of coil shapes, SAR is smaller at a low frequency than at a higher frequency. Furthermore, the simulated results obtained are experimentally validated through the air and boneless pork tissue mediums. The overall PTE and actual power delivered to the implantable coil are also measured. For the future work, a mm-sized implantable coil operating at 13.56 MHz will be designed and fabricated to achieve a high PTE and the wireless link will be tested on freely moving small animals.

Author Contributions: K.M. conceived, designed the study, gave the theoretical and simulation analysis; K.M. and Y.P. designed the coils and carried out the experiments; K.M. and Y.P. revised the whole manuscript; J.R.C. provided guidance and key suggestions for the system design and testing; K.M. wrote the paper.

Funding: This research was supported by the Basic Science Research Program through the National Research Foundation of Korea (NRF) funded by the Ministry of Education, Science and Technology (Grant No. NRF-2016R1D1A3A03918084).

Conflicts of Interest: The authors declare no conflict of interest.

References

1. Jow, U.M.; Ghovanloo, M. Design and optimization of printed spiral coils for efficient transcutaneous inductive power transmission. *IEEE Trans. Biomed. Circuits Syst.* **2007**, *1*, 193–202. [CrossRef] [PubMed]
2. RamRakhyani, A.K.; Mirabbasi, S.; Chiao, M. Design and optimization of resonance-based efficient wireless power delivery systems for biomedical implants. *IEEE Trans. Biomed. Circuits Syst.* **2011**, *5*, 48–63. [CrossRef] [PubMed]
3. Ma, A.; Poon, A.S.Y. Midfield wireless power transfer for bioelectronics. *IEEE Circuits Syst. Mag.* **2015**, *15*, 54–60. [CrossRef]
4. Ahn, D.; Ghovanloo, M. Optimal design of wireless power transmission links for millimeter-sized biomedical implants. *IEEE Trans. Biomed. Circuits Syst.* **2016**, *10*, 125–137. [CrossRef] [PubMed]
5. Agarwal, K.; Jegadeesan, R.; Guo, Y.X.; Thakor, N.V. Wireless power transfer strategies for implantable bioelectronics. *IEEE Rev. Biomed. Eng.* **2017**, *10*, 136–161. [CrossRef] [PubMed]
6. Ha, D.; Lee, T.C.; Weber, D.J.; Chappell, W.J. Power distribution to multiple implanted sensor devices using a multiport bandpass filter (BPF) approach. In Proceedings of the 2014 IEEE MTT-S International Microwave Symposium (IMS2014), Tampa, FL, USA, 1–6 June 2014.
7. Poon, A.S.Y.; O'Driscoll, S.; Meng, T.H. Optimal operating frequency in wireless power transmission for implantable devices. In Proceedings of the 2007 29th Annual International Conference of the IEEE Engineering in Medicine and Biology Society, Lyon, France, 22–26 August 2007.
8. Chang, T.C.; Weber, M.; Charthad, J.; Nikoozadeh, A.; Yakub, P.T.K.; Arbabian, A. Design of high-efficiency miniaturized ultrasonic receivers for powering medical implants with reconfigurable power levels. In Proceedings of the 2015 IEEE International Ultrasonics Symposium (IUS), Taipei, Taiwan, 21–24 Octorber 2015.
9. Schormans, M.; Valente, V.; Demosthenous, A. Practical inductive link design for biomedical wireless power transfer: A tutorial. *IEEE Trans. Biomed. Circuits Syst.* **2018**, *12*, 1112–1130. [CrossRef] [PubMed]
10. Jia, Y.; Mirbozorgi, S.A.; Wang, Z.; Hsu, C.C.; Madsen, T.E.; Rainnie, D.; Ghovanloo, M. Position and orientation insensitive wireless power transmission for enercage-homecage system. *IEEE Trans. Biomed. Eng.* **2017**, *64*, 2439–2449. [CrossRef]
11. Agrawal, D.R.; Tanabe, Y.; Weng, D.; Ma, A.; Hsu, S.; Liao, S.Y.; Zhen, Z.; Zhu, Z.Y.; Sun, C.; Dong, Z.; et al. Conformal phased surfaces for wireless powering of bioelectronic microdevices. *Nat. Biomed. Eng.* **2017**, *1*, 1–9. [CrossRef] [PubMed]

12. Mutashar, S.; Hannan, M.A.; Samad, S.A.; Hussain, A. Analysis and optimization of spiral circular inductive coupling link for bio-implanted applications on air and within human tissue. *Sensors* **2014**, *14*, 11522–11541. [CrossRef]
13. Kiani, M.; Jow, U.M.; Ghovanloo, M. Design and optimization of a 3-coil inductive link for efficient wireless power pransmission. *IEEE Trans. Biomed. Circuits Syst.* **2011**, *5*, 579–591. [CrossRef]
14. Yao, Y.; Meng, X.; Tsui, C.Y.; Ki, W.H. Polyimide-based flexible 3-coil inductive link design and optimization. In Proceedings of the 2018 IEEE Asia Pacific Conference on Circuits and Systems (APCCAS), Chengdu, China, 26–30 Octorber 2018.
15. Mirbozorgi, S.A.; Yeon, P.; Ghovanloo, M. Robust wireless power transmission to mm-sized free-floating distributed implants. *IEEE Trans. Biomed. Circuits Syst.* **2017**, *11*, 692–702. [CrossRef] [PubMed]
16. Christ, A.; Douglas, M.; Nadakuduti, J.; Kuster, N. Assessing human exposure to electromagnetic fields from wireless power transmission systems. *Proc. IEEE* **2013**, *101*, 1482–1493. [CrossRef]
17. Ho, J.S.; Yeh, A.J.; Neofytou, E.; Kim, S.; Tanabe, Y.; Patlolla, B.; Beygui, R.E.; Poon, A.S.Y. Wireless power transfer to deep-tissue microimplants. *PNAS* **2014**, *111*, 7974–7979. [CrossRef] [PubMed]
18. Song, L.; Samii, Y.R. An end-to-end implanted brain–machine interface antenna system performance characterizations and development. *IEEE Trans. Antennas Propag.* **2017**, *65*, 3399–3408. [CrossRef]
19. Manoufali, M.; Bialkowski, K.; Mohammed, B.J.; Mills, P.C.; Abbosh, A. Near-field inductive-coupling link to power a three-dimensional millimeter-sze antenna for brain implantable medical devices. *IEEE Trans. Biomed. Eng.* **2018**, *65*, 4–14. [CrossRef] [PubMed]
20. Yeon, P.; Mirbozorgi, S.A.; Ash, B.; Eckhardt, H.; Ghovanloo, M. Fabrication and microassembly of a mm-sized floating probe for a distributed wireless neural interface. *Micromachines* **2016**, *7*, 154. [CrossRef]
21. Mutashar, S.; Hannan, M.A.; Samad, S.A.; Hussain, A. Design of spiral circular coils in wet and dry tissue for bio-implanted micro-system applications. *Prog. Electromagn. Res.* **2013**, *32*, 181–200. [CrossRef]
22. Zhang, J.; Yuan, X.; Wang, C.; He, Y. Comparative analysis of two-coil and three-coil structures for wireless power transfer. *IEEE Trans. Power Electron.* **2017**, *32*, 341–352. [CrossRef]
23. Zhong, W.X.; Zhang, C.; Liu, X.; Hui, S.Y.R. A methodology for making a three-coil wireless power transfer system more energy efficient than a two-coil counterpart for extended transfer distance. *IEEE Trans. Power Electron.* **2015**, *30*, 933–942. [CrossRef]
24. Mirbozorgi, S.A.; Gosselin, B.; Sawan, M. A transcutaneous power transfer interface based on a multicoil inductive link. In Proceedings of the 2012 Annual International Conference of the IEEE Engineering in Medicine and Biology Society, San Diego, CA, USA, 28 August–1 September 2012; pp. 1659–1662.
25. Nair, V.V.; Choi, J.R. An efficiency enhancement technique for a wireless power transmission system based on a multiple coil switching technique. *Energies* **2016**, *9*, 156. [CrossRef]
26. Soma, M.; Galbraith, D.C.; White, R.L. Radio-frequency coils in implantable devices: Misalignment analysis and design procedure. *IEEE Trans. Biomed. Eng.* **1987**, *BME-34*, 276–282. [CrossRef]
27. Huang, W.; Ku, H. Analysis and optimization of wireless power transfer efficiency considering the tilt angle of a coil. *J. Electromagn. Eng. Sci.* **2018**, *18*, 13–19. [CrossRef]
28. Khan, S.R.; Choi, G.S. Analysis and optimization of four-coil planar magnetically coupled printed spiral resonators. *Sensors* **2016**, *16*, 1219. [CrossRef]
29. Sun, G.; Muneer, B.; Li, Y.; Xhu, Q. Ultracompact implantable design with integrated wireless power transfer and RF transmission capabilities. *IEEE Trans. Biomed. Circuits Syst.* **2018**, *12*, 281–291. [CrossRef]
30. Dielectric Properties of Body Tissues. Available online: http://niremf.ifac.cnr.it/tissprop/htmlclie/htmlclie.php (accessed on 15 July 2018).
31. Yellappa, P.; Lee, Y.R.; Choi, J.R. Analysis of coil misalignment issue in resonance-based wireless power transmission system for implantable biomedical applications. In Proceedings of the 2018 IEEE International Symposium on Circuits and Systems (ISCAS), Florence, Italy, 27–30 May 2018.
32. Jow, U.M.; Ghovanloo, M. Modeling and optimization of printed spiral coils in air, saline, and muscle tissue environments. *IEEE Trans. Biomed. Circuits Syst.* **2009**, *3*, 339–347.

33. Xue, F.; Cheng, K.W.; Je, M. High-efficiency wireless power transfer for biomedical implants by optimal resonant load transformation. *IEEE Trans. Biomed. Circuits Syst.* **2013**, *60*, 867–874. [CrossRef]
34. Yang, C.L.; Chang, C.K.; Lee, S.Y.; Chang, S.J.; Chiou, L.Y. Efficient four-coil wireless power transfer for deep brain stimulation. *IEEE Trans. Microw. Theory Tech.* **2017**, *65*, 2496–2507. [CrossRef]